Materials Today Chemistry 26 (2022) 101122

Contents lists available at ScienceDirect

Materials Today Chemistry

journal homepage: www.journals.elsevier.com/materials-today-chemistry/

Phenolic compounds as redox-active exfoliation agents for group VI transition metal dichalcogenides

D. Rojas [a], F. Della Pelle [a, *], F. Silveri [a], G. Ferraro [b], E. Fratini [b], D. Compagnone [a, **]

[a] Faculty of Bioscience and Technology for Food, Agriculture and Environment, University of Teramo, Campus "Aurelio Saliceti" Via R. Balzarini 1, 64100 Teramo, Italy

[b] Department of Chemistry "Ugo Schiff" and CSGI, University of Florence, Via Della Lastruccia 3-Sesto Fiorentino, I-50019, Florence, Italy

ARTICLE INFO

Article history:
Received 18 May 2022
Received in revised form
31 July 2022
Accepted 1 August 2022
Available online xxx

Keywords:
2D materials
Van der Waals materials
Functional materials
Hybrid organic/inorganic nanomaterials
Functional phytocompounds
Liquid phase exfoliation

ABSTRACT

Simple, cheap, and green exfoliation methods for the mass production of two-dimensional (2D) nanomaterials are still required for their widespread adoption. In this context, this work presents a systematic study regarding the exfoliation of group VI transition metal dichalcogenides (TMDs) using 14 different food-derived phenolic compounds of different structural complexity. Phenolic compounds have demonstrated to successfully assist the liquid phase exfoliation conferring unique redox functionalities to the TMDs nanosheets. The most performant exfoliating agents have been carefully optimized and demonstrated to produce stable 2D nanoflakes dispersions with peculiar electrochemical properties. This work proves how properly selected natural stabilizing agents allow an effective TMDs exfoliation, giving rise to hybrid organic/inorganic nanomaterials with functional electrochemical and additional catalytic features. The reported approach opens new paths for the green production of exfoliated 2D functional nanomaterials for sensing, biosensing, and energy applications.

1. Introduction

Two-dimensional (2D) layered materials and their heterostructures represent one of the most promising forefronts in the nanomaterial field. These materials show quite different structures with respect to the carbon 2D honeycomb lattice of graphene, offering additional and unexpected properties related to their peculiar chemical composition and physical state; this often allows to go beyond graphene opportunities [1,2]. Among 2D layered materials, transition metal dichalcogenides (TMDs) and, in particular, MoS_2, WS_2, $MoSe_2$, and WSe_2 have attracted a worldwide multidisciplinary research interest [3]. TMDs are layered materials with a crystal structure consisting of sheets with a hexagonal layer of metal atoms (M) sandwiched between two layers of chalcogen atoms (Q). The TMDs sheet wafer structure (Q-M-Q) is held together by covalent bonds, while van der Waals interactions occur between adjacent Q-M-Q sheets [4,5]. The TMDs versatile chemistry results particularly appealing in several fields, including catalysis and energy storage, sensing, biosensing, and device realization [6] as well as for biological/biomedical applications [5,7]. The TMDs exfoliation is crucial to tailor the final properties of the material, such as the number of layers, dimension, solubility, and reactivity [6,8]. In this regard, impressive efforts have been devoted to improve physical and chemical processes to obtain few-layered TMDs with tailored properties.

The exfoliation of bulk TMDs to monolayer or few layers nanosheets requires the breaking of the weak Van der Waals interactions existing between adjacent layers in the pristine form. The exfoliation increases the exposed area and edge atoms, leading to higher reactivity and catalytic activity, and affecting electronic, photonic, and magnetic properties [9–11]. Mechanical and chemical exfoliation, as well as chemical vapor deposition and chemical synthesis starting from precursors, are the conventional techniques to obtain a few-layered TMDs-controlled structure [5]. Among others, TMDs Li intercalation followed by a further exfoliation represents one of the most used techniques to obtain water-soluble single-layer TMDs in the metastable trigonal symmetry (1T) where the atoms present octahedral coordination [5,12]. On the other hand, direct liquid phase exfoliation (LPE) assisted by controlled ultrasounds has become an affordable large-scale approach to produce few-layered hexagonal TMDs (2H) with the prismatic coordination of transition metal atoms [11,13]. LPE has been mainly studied in

* Corresponding author.
** Corresponding author.
E-mail addresses: fdellapelle@unite.it (F. Della Pelle), dcompagnone@unite.it (D. Compagnone).

https://doi.org/10.1016/j.mtchem.2022.101122
2468-5194/

organic solvents that act as dispersing and stabilizing phases [14,15]; however, the real challenge is to apply this exfoliation in water preserving the characteristics of the material. 2D TMDs nanocolloids in aqueous medium have been obtained via LPE using different stabilizing agents, such as surfactants, polymers, and other amphiphilic compounds, mainly acting through non-covalent interactions [11]. Recently, Griffin et al. have studied a broad range of common surfactants, demonstrating how the surfactant type and concentration affect the dimension and conformation of the nanosheets [16].

Motivated by the ongoing chemical green revolution and the United Nations sustainable development goals [17], the use of low-impact materials, biomolecules, phytochemicals, and by-products has burst also in the materials and applied science scenario [18–20]. In this regard, proteins, peptides, nucleotides, and bile salts have been demonstrated to be able to assist 2D materials exfoliation [21,22]. Recently, also natural products have been used for the same aim (i.e. polysaccharides, parts of plants, extracts, etc.). Among phytochemicals, phenolic compounds (PCs) are useful tools in the nanomaterial domain, beyond their conventional role of antioxidant and healthy compounds. PCs can act as stabilizers, inducing self-assembly, and/or stabilizing PCs-functionalized nano- and micro-structures [23–25]. The intimate interaction among catechols-containing PCs and nanomaterials has been recently reviewed by Size-Posey et al. [26], while the PCs' role as building blocks to generate supramolecular nanostructure and microstructure has been recently proven [27,28], definitely endorsing the potential technological role of PCs.

PCs-rich plant extracts and some pure PCs have been used for graphene oxide reduction [29], while few papers describe their use for direct graphite exfoliation [30–32]. Exfoliation of MoS_2 was attempted using tannic acid, a branched soluble tannin chosen for the high charge/mass ratio and for the well-recognized ability to act as a stabilizer; also, tea catechins have been tested for the exfoliation of TMDs. The obtained nanosheets were employed for chemical 4-nitrophenol reduction [33], as nanocarriers for antibiotic drugs [34], as nanofillers for advanced filters [35], additives for batteries [36], and flame-retardants [37]. Despite, PC-functionalized carbon nanomaterials having demonstrated captivating electrochemical activities [38–41], to the best of our knowledge, no systematic investigation to understand the role of PCs in the TMDs liquid phase exfoliation is present.

In this work, natural phenols compounds' ability to assist the TMDs exfoliation and the electrochemistry of the obtained nanosheets were studied in detail. Initially, the MoS_2 exfoliation has been attempted by using fourteen naturally derived PCs, ranging from simple phenols to more complex structures. The exfoliation has been studied under increasing concentrations of polyphenols and physicochemical features of the obtained nanosheets have been investigated to highlight the role of PCs in this process. The electrochemistry of the PCs-stabilized TMDs nanosheets has been then characterized to understand the effect of the phytochemical structure employed on the final colloids. Different electrochemical probes have been tested and different electrocatalytic direct and mediated applications studied to understand the nanosheets electrochemistry and potential catalytic ability. For the most promising PC, i.e. ellagic acid (EA), the exfoliation process has been extended to four TMDs materials of Group VI, i.e. MoS_2, WS_2, $MoSe_2$, and WSe_2. Finally, the four exfoliated TMDs have been characterized, proving useful and unexpected properties. Here we demonstrate how a properly selected natural stabilizing agent allows an effective TMDs exfoliation and structure modification toward a hybrid organic/inorganic nanomaterial with improved electrochemical and catalytic features.

2. Experimental section

2.1. Materials and chemicals

All bulk materials were purchased in powder form (99% purity). The supplier and the dimensions of the TMD studied are as follows: MoS_2 (Sigma-Aldrich, St Louis, MO, USA; <2 μm), WS_2 (Sigma-Aldrich, St Louis MO, USA; <2 μm), $MoSe_2$ (Alfa Aesar, Germany; ~44 μm), WSe_2 (Alfa Aesar, Germany; 10–20 μm). Sodium phosphate monobasic monohydrate, potassium ferrocyanide, potassium ferricyanide, ruthenium hexamine, potassium chloride, sulfuric acid, hydrazine were purchased from Sigma-Aldrich (St Louis, MO, USA). The PCs (Sigma-Aldrich, St Louis, MO, USA) investigated are catechol (CA), p-coumaric acid (CU), caffeic acid (CF), gallic acid (GA), kaempferol (KA), rutin (RU), quercetin (QU), morin (MO), myricetin (MY), catechin (CT), epigallocatechin (EP), ellagic acid (EA), oleuropein (OL), and tannic acid (TA). Milli-Q grade water (Millipore, Bedford, MA, USA) was employed as the continuous medium in the exfoliation procedure and the preparation of the solutions.

2.2. Physicochemical characterization

Visible spectra were recorded using a Perkin Elmer Lambda 25 UV–Vis spectrometer (Perkin Elmer Corp, Baden Seewerk, Germany); the measurements were performed by putting the samples in quartz cuvettes (resolution 1 nm) against blank (water). Scanning electron microscopy (SEM) micrographs were acquired using a ΣIGMA high-resolution scanning electron microscope (Carl Zeiss Microscopy GmbH, Germany). All the experiments were conducted on uncoated samples with an acceleration potential of 2 kV and at a working distance of about 4 mm. Raman spectra were acquired with the Renishaw inVia™ Qontor® confocal Raman microscope equipped with a Leica DM microscope to focus the laser on the sample with a 20× objective (NA 0.40, WD 1.15 mm). All the experiments were performed using the 532 nm laser line (diode-type, Renishaw 80 mW 532 nm edge, 1800 L/mm grating, 10% laser power) after instrument calibration on the internal Si-reference standard (520.5 ± 0.1 cm^{-1}). All the spectra were recorded with a spectral resolution of 1 cm^{-1} in the spectral range between 100 and 3200 cm^{-1} using the static mode (exposure time 10 s).

2.3. Exfoliation strategy

The PCs-assisted exfoliation of MoS_2, WS_2, $MoSe_2$, and WSe_2 was carried out using a probe sonicator Sonifier® SFX550 (Branson, Danbury, Connecticut, USA. Wattage Output: 550 W; frequency Output: 20 kHz), keeping the dispersions in an ice-bath during the process to maintain the temperature below 10 °C. For the PCs screening, exfoliation was conducted by sonicating for 1h 100 mg of MoS_2 in 10 mL of a 1 mg mL^{-1} phenolics water solution. In this case, a tapered microtip (Ø = 13 mm) was used to maximize the power delivery (pulsed program: 2 s ON/1 s OFF, 50% amplitude). Finally, the supernatant was discarded and the TMD sediment was resuspended in 10 mL of Milli-Q water. For the selected PCs, the reaction was scaled up: 0.5 g of TMDs powder were added to 50 mL of an aqueous solution containing the PC and then sonicated for 5 h (pulsed program: 2 s ON/1 s OFF, 50% amplitude). The amount used for each PC was optimized to obtain the maximum yield. The resulting raw TMD dispersion was subjected to a centrifugation step at 250 g for 1 h to remove the unexfoliated material. The sediment was discarded, and the supernatant was further centrifuged at 20,000 g for 15 min to remove the PC excess. Eventually, the supernatant was discarded and the TMD sediment was resuspended in 50 mL of Milli-Q water.

2.4. Electrochemical measurements

The electrochemical measurements were carried out using a Palmsens 4 Potentiostat/Galvanostat/Impedance Analyzer (Palm Instruments BV, Houten, Netherlands). The electrochemical cell was composed of a glassy carbon working electrode (GC) (Ø = 3 mm), an Ag/AgCl (1 M KCl) reference electrode, and a Pt wire as a counter electrode. To explore the electrochemical features of the +PCs-TMDs, the GC surface was modified via drop-casting 5 μL of the PCs-TMDs dispersion at a concentration of 0.2 mg mL^{-1} (1 μg of material). The inherent electrochemistry of PCs-TMDs and PPs in solution was investigated by performing cyclic voltammetry (CV) in 0.1 M phosphate buffer (PB) at pH 7. The electron charge transfer properties of the materials were explored via CVs using two redox probes: 5 mM $[Fe(CN)_6]^{3-/4-}$ and $[Ru(NH_3)_6]^{2+/3+}$ in 0.1 M KCl. Electrochemical impedance spectroscopy (EIS) was performed with 5 mM $[Fe(CN)_6]^{3-/4-}$ using a sinusoidal wave with 5 mV of amplitude centered at the open circuit potential in a frequency range from 10^5 to 10^{-1} Hz.

The electrocatalysis of PCs-TMDs toward hydrazine was demonstrated employing CVs and Chronoamperometry. The CVs were carried out in 0.1 M PB at pH 7 (−0.3 to 0.7 V of potential range, 25 mV s^{-1} of scan rate), whereas chronoamperometry was run under stirring at +0.4 V potential. For the hydrogen evolution reaction (HER) measurements, an Ag/AgCl (1 M KCl) reference electrode, and a Pt wire as a counter electrode were used. Before the measurement, the 0.5 M H_2SO_4 electrolyte was degassed using N_2 gas for 30 min. The linear sweep voltammetry and the Tafel plot analysis were conducted at a scan rate of 5 mV s^{-1}. All the measured potentials were converted to the reversible hydrogen electrode post-analysis using the following equation: reversible hydrogen electrode = Ag/AgCl (V) + 0.059 (pH) + 0.235 V, where the 0.235 V value is the potential of the Ag/AgCl (1 M KCl) reference electrode. The electrochemical measurements were performed three times. The current density was achieved normalizing the current by the geometric area of the electrode.

3. Results and discussion

This work aims to clearly show that PCs are able to act as stabilizing agents during TMDs sonochemical LPE giving, as added value, an improvement of the electrochemical characteristics while limiting, at the same time, the passive and sometimes adverse role of common surfactants. Thus, the influence of the PC structure on the TMDs exfoliation has been studied, and, for the successfully exfoliated materials, the integrated electrochemistry was evaluated to prove their potentiality.

3.1. Influence of the phenol structure on MoS_2 LPE in water

To explore the PC's ability to assist TMDs exfoliation, MoS_2 has been chosen as model substrate in the presence of different PCs, ranging from small molecules, as catechol, to complex structures, as tannic acid. Fig. 1 reports the chemical structures of the investigated PCs, together with a histogram ranking the PCs exfoliation achieved (expressed as the optical density at 670 nm, taken as exfoliation screening index) and the visual appearance of the MoS_2 dispersions after sonication. This exfoliation to screen PCs was conducted according to Section 2.3.

Fig. S1 reports the spectra of the MoS_2 obtained dispersions in the characteristic visible region.

The data obtained indicate that polyphenols are more active compared with simple phenols (i.e. CA, CU, and GA). The only exception is CF, which exhibits some ability to assist MoS_2 exfoliation, probably for the additional charge of the carboxylic moieties and for the well-known polymerization ability [42]. Among flavonols, KA, RU, and QU are not able to assist the exfoliation, while MY and MO are active. This behavior could not be only attributed attributed to the different hydroxy positions on the structures of the molecules but also to their different solubility in water [43,44]. Looking at the behavior of flavanols, where CT is more active than EP, it is possible to exclude that the only key factor for exfoliation lies in the number of hydroxyls. Indeed, catechin (CT) is one of the polyphenols where polymerization is more studied and occurs also spontaneously [45]; this may play some role. In the case of OL and TA, the complexity of the structure and the high number of hydroxylic groups justify their exfoliating capacity; on the other hand, the EA results particularly active probably for the planar/flat structure and the conjugation of 2 aromatic rings and 2 lactones, which allows sheets intercalation [46] and minimize the charge repulsion during stacking with the TMDs sheet. Interestingly, PCs besides being amphiphilic compounds can give rise to polymerization reactions [47], potentially promoting their ability to interact and adhere with nanomaterial surfaces [48,49]; this behavior has been particularly observed for catechol-containing structures [50].

3.2. Natural phenols-mediated MoS_2 LPE mechanism. Hypothesis and characterization

To maximize yields from each PC and understand their role in the LPE process, the influence of PC concentration was studied for the five PCs giving a higher yield of exfoliated MoS_2 i.e. catechin (*CT*-MoS_2), ellagic acid (*EA*-MoS_2), morin (*MO*-MoS_2), oleuropein (*OL*-MoS_2), and tannic acid (*TA*-MoS_2). The exfoliation was carried out following the protocol described in section 2.3.

In Fig. S2, it is possible to appreciate the different behavior obtained for the different polyphenols; the amount of exfoliated MoS_2 increases with the PC amount, indicating their active role, reaching a plateau and/or decreasing depending on the chemical structure and consequent PC/substrate and PC/PC interactions. The reaching of a plateau or decreasing in yield has been observed for conventional surfactants and is attributed to the presence of the critical micellar concentration [13]. In this case, it can be due to a combination of a critical concentration for the aggregation, intrinsic solubility, surface reactivity/saturation, and intermolecular forces. Depending on the PC structure, after the maximum MoS_2 flakes surface covering/exfoliation, the increase in the PC in solution can favor the TMD aggregation as a result of the staking process causing a decrease of the yield.

To better understand the mechanism behind PC-mediated exfoliation of TMDs, CT and EA have been selected as case studies; they have similar molecular weight but different chemical structures and exfoliating abilities. The amount of PC adsorbed on the exfoliated TMD was quantified as a function of PC initial concentration. Fig. 2 reports the trend of the adsorbed PC expressed as $m^2\ g^{-1}$ and calculated dividing the surface area of adsorbed PC molecules (their cross-section was calculated using DataWarrior software [51]) by the weight of the exfoliated MoS_2 as a function of PC concentration used in the exfoliation procedure. The same graph also shows the MoS_2 amount changes after exfoliation vs. the PC concentration used.

It can be observed that EA (▲) is more efficient in the exfoliation of MoS_2 in comparison with CT (•) at the concentration of 1 mg mL^{-1} (i.e. 3.3 and 3.4 mM for CT and EA, respectively). This behavior is linked to the preferential adsorption of the planar and rigid structure of EA that results in a greater intercalation ability [52], in contrast to the more flexible CT structure, rather than their different cross-sections (93 $Å^2$ and 100 $Å^2$ for EA and CT, respectively, as calculated using DataWarrior [53]).

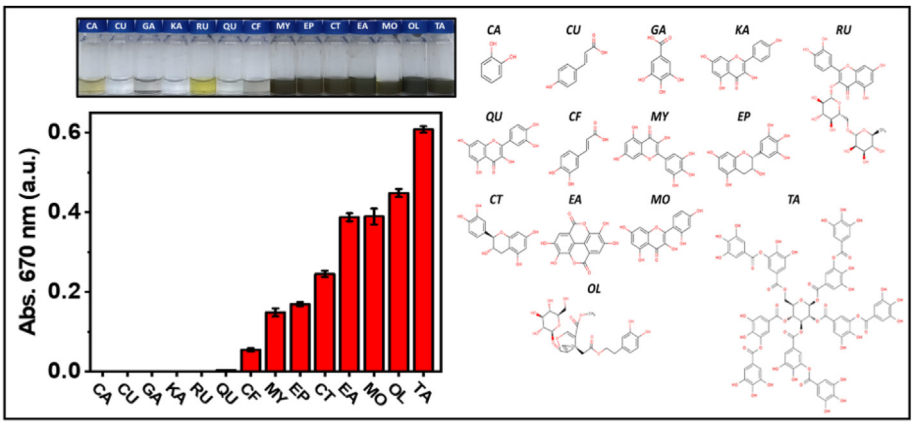

Fig. 1. Left: absorbance at 670 nm of MoS_2 dispersions obtained by LPE assisted by various types of phenolic compounds. Data reported as mean value of n = 3 independent exfoliations, RSD ≤7 %. The picture above the bar chart reports the picture of the MoS_2 dispersions with the acronym of the phenolic compound used for the exfoliation. Right: Chemical structures of the phenolic compounds used in this study. Catechol (CA), p-coumaric acid (CU), gallic acid (GA), kaempferol (KA), rutin (RU), quercetin (QU), caffeic acid (CF), myricetin (MY), epigallocatechin (EP), catechin (CT), ellagic acid (EA), morin (MO), oleuropein (OL), and tannic acid (TA). LPE, liquid phase exfoliation.

Further increasing PC concentration up to 10 mM, the amount of adsorbed polyphenol increases for both molecules. The exfoliation yield remains constant for CT while significantly decreases in the case of EA for PC concentrations higher than 8 mM. This observation suggests preferential polyphenol–polyphenol interactions at high PC amounts, particularly for EA. This behavior can be attributed to π-π interactions among EA molecules adsorbed on the flakes and EA molecules in solution which cause the re-aggregation of exfoliated flakes and a decrease in MoS_2 yield. On the contrary, the less rigid conformation of the catecholic moiety of CT and the low conjugated structure results in a lower tendency to promote PC–PC re-staking. A similar trend in the exfoliation yield is observed at high PC concentration also for OL and MO (Fig. S2), which possess a structure similar to CT.

The *PCs*–MoS_2 dispersions obtained, with the optimal PC concentration (i.e. the amount that maximizes the exfoliation yield), were then characterized using Visible and Raman spectroscopy and SEM. Fig. 3A reports the visible spectra of the different *PCs*–MoS_2. In all cases, the spectra show two different peaks denominated as A and B excitons attributed to the direct excitonic transitions of MoS_2 characteristic of the 2H-phase [54,55]. Interestingly, Fig. S3A confirms the EA interaction on the MoS_2 surface; indeed, the *EA*-MoS_2 spectrum exhibits the typical peaks of the exfoliated MoS_2 and the characteristic peaks of the EA in solution. Fig. 3B collects the Raman spectra of the different MoS_2 nanomaterials. The spectra clearly evidence two vibration modes, the in-plane (E^1_{2g}) and out-of-plane (A_{1g}) vibration modes around 380 and 405 cm^{-1}, respectively [56]. Our data show that the positions for the bulk MoS_2 are 374.1 cm^{-1} and 401.8 cm^{-1}, whereas all *PCs*–MoS_2 nanosheets exhibit a blue shift of both A_{1g} and E^1_{2g} vibration modes. This shift has been attributed to the suppression of atom vibration induced by the intermolecular force and Coulombic force caused by the chemical groups absorbed on the MoS_2 nanosheets [57].

Fig. 4 shows the SEM micrographs of the bulk-MoS_2, and the exfoliated *CT*-MoS_2, *EA*-MoS_2, *MO*-MoS_2, *OL*-MoS_2, and *TA*-MoS_2.

SEM micrographs reveal that the PC-assisted exfoliated flakes result significantly smaller than the bulk MoS_2 as a result of a successful exfoliation. The co-presence of structures with morphology not ascribable to the classical flakes' arrangement of TMD materials (i.e. globular or necklace structures) can be the result of the polymerization of PCs induced by the sonication treatment as already reported in the literature [58–60]. To further characterize the colloidal properties and dimensions of the *PCs*–MoS_2 nanosheets, z-potential and dynamic light scattering measurements were carried out (Fig. S4). The surface z-potential for each nanosheet were −36 ± 1 mV *CT*-MoS_2, -52 ± 1 mV *EA*-MoS_2, -45 ± 1 mV *MO*-MoS_2, -48 ± 2 mV *OL*-MoS_2, and -41 ± 1 mV *TA*-MoS_2. The difference among materials reflects the different

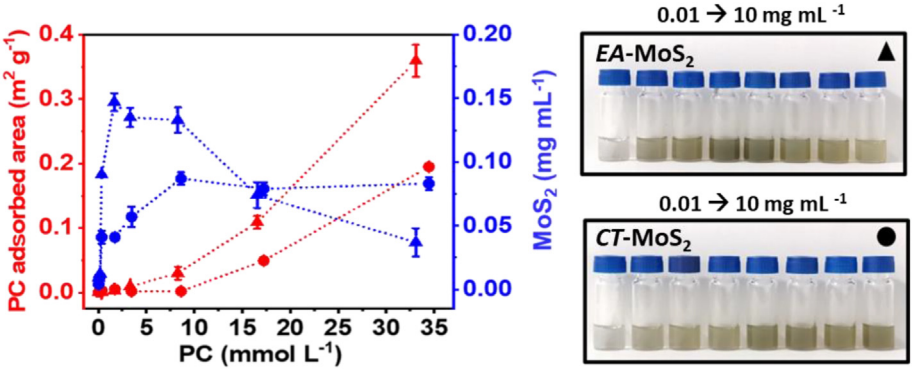

Fig. 2. Adsorbed PC expressed as $m^2\ g^{-1}$ calculated considering the cross-section of the adsorbed molecule divided by the weight of the exfoliated MoS_2 (red) and the MoS_2 amount as a function of the initial concentration of PC used in the exfoliation procedure (blu). Data reported as mean value of n = 3 independent exfoliations. Legend: ▲ = *EA*-MoS_2; ● = *CT*-MoS_2. Right panel: pictures of the MoS_2 dispersions obtained with increasing amounts of EA and CT.

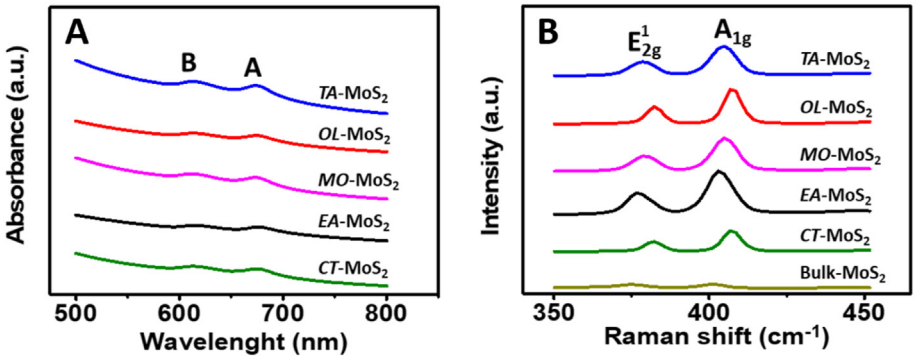

Fig. 3. (**a**) Visible absorption and (**b**) Raman spectra of MoS_2 exfoliated by LPE employing the optimal concentration of the phenolic compounds able to act as stabilizing agents. LPE, liquid phase exfoliation.

surface charges due to the adsorbed PCs. Dynamic Light Scattering analysis gave size values as 153 ± 2 nm for *CT*-MoS_2, 165 ± 3 nm for *EA*-MoS_2, 144 ± 2 nm for *MO*-MoS_2, 158 ± 1 nm for *OL*-MoS_2 and 125 ± 2 nm for *TA*-MoS_2. The size was quite similar among the different PCs being the smallest size obtained with the *TA*-MoS_2.

3.3. Electrochemistry of MoS_2. Influence of the employed natural phenol and catalytic properties

The influence of the PCs-assisted exfoliation in the electrochemistry of MoS_2 nanosheets was first studied by modifying by drop-casting a GCE with the different *PCs*—MoS_2 dispersions first brought to the same concentration (0.2 mg/mL). The electrodes were immersed in PB (pH = 7) and the inherent electrochemical signals of the electrode were recorded. As can be seen in Fig. 5, each material exhibits a different pattern in the voltammogram which is related to the different surface composition. To have further insight into the electrochemical process, the signal is compared to the corresponding polyphenol in solution recorded at a bare GC electrode.

Interestingly, the electrochemical signal of the *PCs*—MoS_2 is characterized by a shoulder in the proximity of the anodic peak of the respective PC; the slight anodic shift of the shoulder can be attributed to the formation of an adduct on the MoS_2. These results demonstrate that the proposed exfoliated method can transfer the inherent electrochemistry of the PC used in the assisted LPE to the exfoliated material. This behavior has not been observed for the *OL*-MoS_2. While for the *EA*-MoS_2, it is interesting to note that the chemistry of the EA observed in solution is practically totally maintained even after adhesion on the MoS_2 flakes. This suggests that the EA adhered to the nanoflakes does not undergo significant structural changes, preserving the redox-active moieties. Finally, the ultrasound treatment effect on the PC in solution was studied; to this aim, EA in solution was subjected to exfoliation treatment in the absence of bulk-MoS_2. In Fig. S3B, it is possible to observe how the sonochemical treatment does not affect the EA electrochemistry, suggesting that the molecule does not undergo significant structural changes.

To further explore the interfacial electrochemical properties of the *PCs*—MoS_2 nanosheets, $[Fe(CN)_6]^{4-/3-}$ was used as inner sphere redox probe. CV and EIS were used as characterization techniques and the results are collected in Fig. S5.

As shown in Figs. S5A and B, the *EA*-MoS_2 nanosheets exhibit the worst electrochemical behavior having the lowest heterogeneous electron transfer rate k^o corresponding to 2.78×10^{-6} ($\pm 1.16 \times 10^{-6}$) cm s^{-1}. Similar k^o were found for *TA*-MoS_2, *MO*-MoS_2, and *CT*-MoS_2 with values of 3.26×10^{-6} ($\pm 6.27 \times 10^{-7}$), 3.29×10^{-6} ($\pm 5.11 \times 10^{-7}$), and 3.45×10^{-6} ($\pm 1.09 \times 10^{-6}$) cm s^{-1}, respectively. Heterogeneous electron transfer was the highest for *OL*-MoS_2 with a value of 4.00×10^{-6} ($\pm 9.16 \times 10^{-7}$) cm s^{-1}. A similar trend with the electrochemical performance is observed in the EIS data. The charge transfer resistance value (R_{CT}) at the

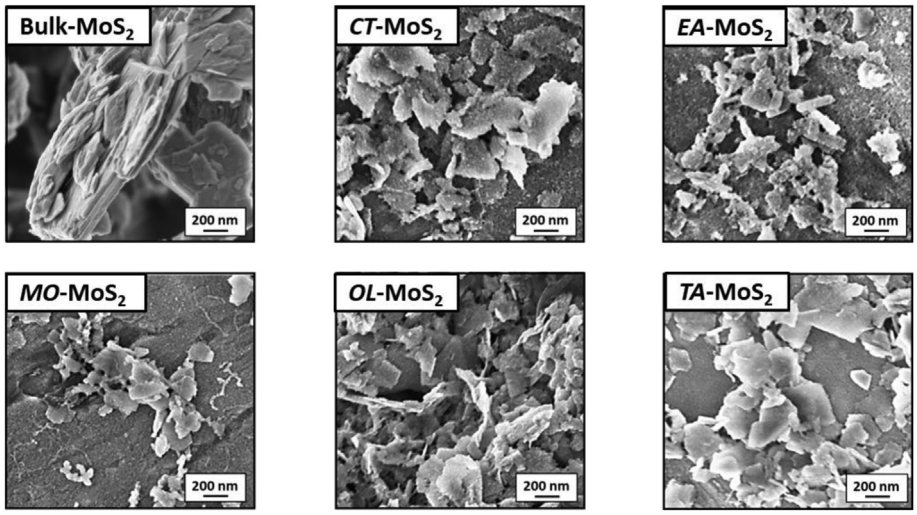

Fig. 4. SEM micrographs of the native MoS_2 (bulk-MoS_2) and the MoS_2 exfoliated with different phenolic compounds, i.e. catechin (*CT*-MoS_2), ellagic acid (*EA*-MoS_2), morin (*MO*-MoS_2), oleuropein (*OL*-MoS_2), and tannic acid (TA-MoS_2) at the same magnification (100 kX). SEM, scanning electron microscopy.

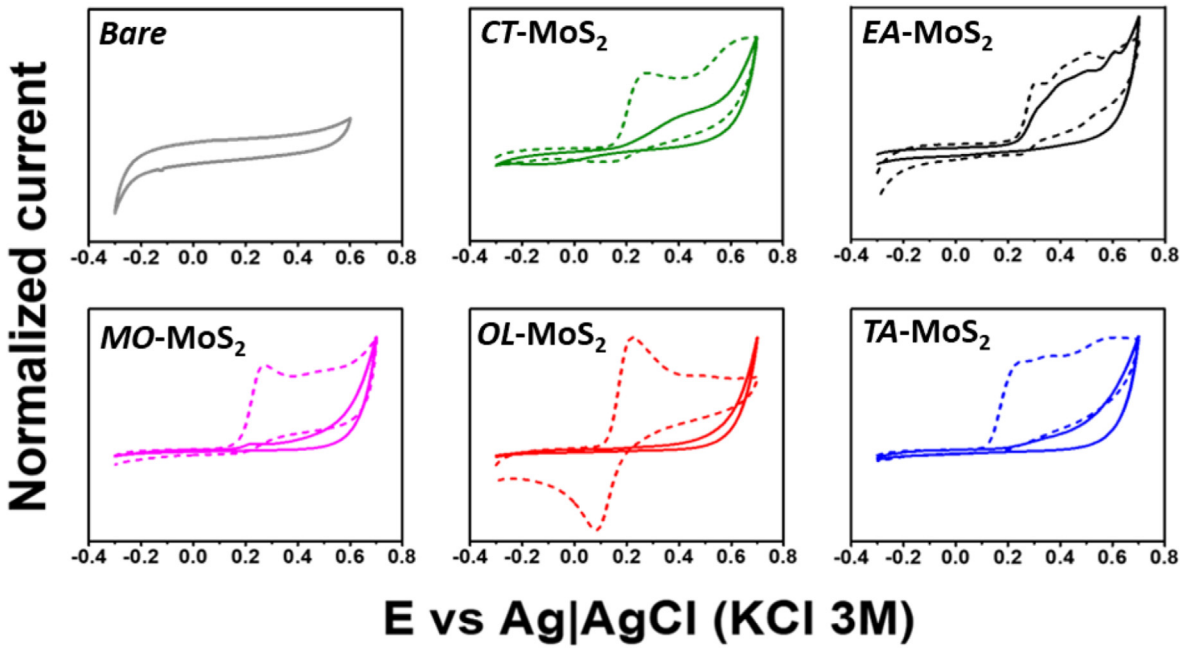

Fig. 5. Dashed lines: cyclic voltammograms of 100 μM PC (i.e. CT, EA, MO, OL, and TA) in phosphate buffer (pH = 7) using GC electrode. Solid lines: cyclic voltammograms of the GC electrodes modified with the same amount of *PCs*—MoS_2 dispersion (i.e. *CT*-MoS_2, *EA*-MoS_2, *MO*-MoS_2, *OL*-MoS_2, and *TA*-MoS_2), in phosphate buffer (pH = 7). All the CVs were conducted at a scan rate of 25 mV s^{-1}. CT, catechin; CV, cyclic voltammetry; EA, ellagic acid; GC, glassy carbon; MO, morin; OL, oleuropein; TA, tannic acid.

electrode surface was extracted from the EIS spectra by fitting the experimental data to the classical Randles equivalent circuit. The obtained values were 9.04 ± 1.45, 6.87 ± 1.70, 5.63 ± 0.95, 4.21 ± 0.37, and 4.10 ± 0.62 kΩ for *EA*-MoS_2, *MO*-MoS_2, *TA*-MoS_2, *CT*-MoS_2, and *OL*-MoS_2. From these data, we can conclude that *EA*-MoS_2 exhibits the poorest performance and *OL*-MoS_2 shows the best performance while a similar performance is obtained for *MO*-MoS_2, *TA*-MoS_2, and *CT*-MoS_2. Interestingly, the data fit well with the intensity of the signal due to the inherent electrochemistry of the *PCs*—MoS_2 electrodes, where the highest signal is obtained by the EA residues in *EA*-MoS_2; whereas in the *OL*-MoS_2, there is not a visible faradaic process. For the *MO*-MoS_2, *TA*-MoS_2 and *CT*-MoS_2 residual current is still visible but with lower intensity than *EA*-MoS_2. The highest inherent electrochemical signal indicates a higher coverage of the material, which hinders the electronic transfer of the inner sphere redox probe; it is widely known that food polyphenols are able to cause fouling of electrode surfaces [61–66].

To confirm the hypothesis an experimental control using $[Ru(NH_3)_6]^{2+/3+}$, an outer sphere redox probe insensitive to the surface functional groups was carried out [67]. As shown in Fig. S6, no significant differences in the peak separation were observed between the different *PCs*—MoS_2, and slight differences in the peak intensity are observed that can be attributed to small changes in the area of the electrodes. Thus, electron transfer is similar (same peak separation) and no significantly different electrochemical surface area among electrodes was found because of the similar peak intensity.

As a practical application to the proposed LPE, the nanosheets were tested for N_2H_4 oxidation, a reaction known to be electrocatalyzed by hydroxylic/quinonic groups [68,69]. Hydrazine oxidation is an important reaction since it is employed in the anode of direct hydrazine fuel cells. Direct hydrazine fuel cells offer advantages like the use of liquid-type fuels that facilitate their transformation, storage, and supply, and zero carbon emission systems in the electrochemical conditions used [70]. In addition, hydrazine is a widely known carcinogen agent, and therefore, its determination at a low concentration level is also a major concern.

Fig. 6 reports the electrochemical signal obtained in PB pH 7 and in the presence of 5 mM of N_2H_4.

The pattern of the signals is very different in the case of EA compared with the other PCs. In the case of EA, a peak in the same potential region of the *EA*-MoS_2 but with much higher current intensity was achieved. This is a classical behavior for mediated oxidation, suggesting that *EA*-related compounds rich in hydroxylic groups present in the surface can mediate the electrochemical oxidation of N_2H_4. In contrast, the other PCs exhibit lower currents, 7.5 ± 0.5, 13.2 ± 0.9, 19.4 ± 1.5, and 21.1 ± 1.3 μA for *TA*-MoS_2, *CT*-MoS_2, *MO*-MoS_2, and *OL*-MoS_2, respectively, with respect to the 76.3 ± 4.3 μA for EA, measured at +0.4 V vs Ag|AgCl. In the case of non-EA PCs, the electrochemical signal shape is different from the inherent signal suggesting that the mediated oxidation is negligible. For comparison, the oxidation of N_2H_4 in a bare GC electrode is reported and just a very small oxidation current (0.6 ± 0.1 μA) is observed.

The electrochemical characterization performed for the different *PCs*—MoS_2 points to the *EA*-MoS_2 as a functional material with a higher PC coverage, and the ability to mediate the oxidation of N_2H_4. In addition, even if higher exfoliation yield is obtained using TA and similar yields are obtained with MO and OL, the electrochemical performance obtained with EA is significantly superior. Therefore, this PC was selected to further study the exfoliation of other TMDs belonging to group VI of the periodic table. The *EA*-MoS_2 higher performance can be attributed to the EA preserved electrochemistry, which is maintained also after adhesion to the MoS_2 nanoflakes.

3.4. Electrochemistry of group VI TMDs. Electrochemical oxidation of N_2H_4

EA has been used also to exfoliate the others group VI TMDs. Good exfoliation performance, comparable to that obtained with

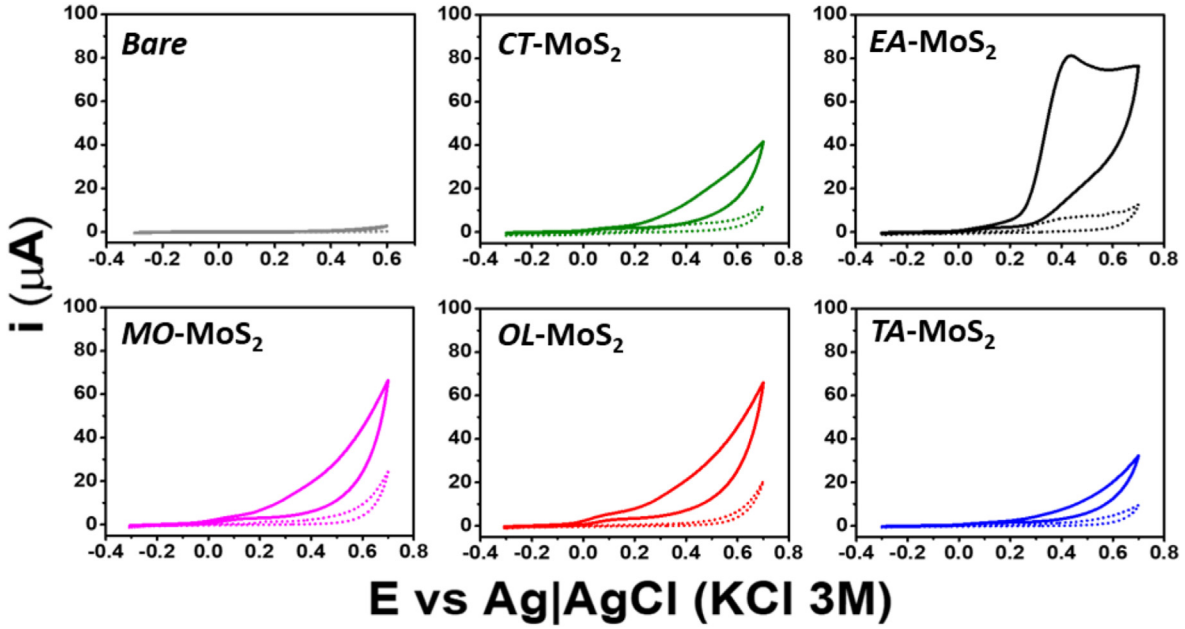

Fig. 6. CVs of MoS_2 exfoliated with different PCs in a blank phosphate buffer solution (dashed line) and containing 5 mM of N_2H_4 (solid line). (Scan rate: 25 mV s^{-1};pH: 7). CV, cyclic voltammetry; PC, phenolic compound.

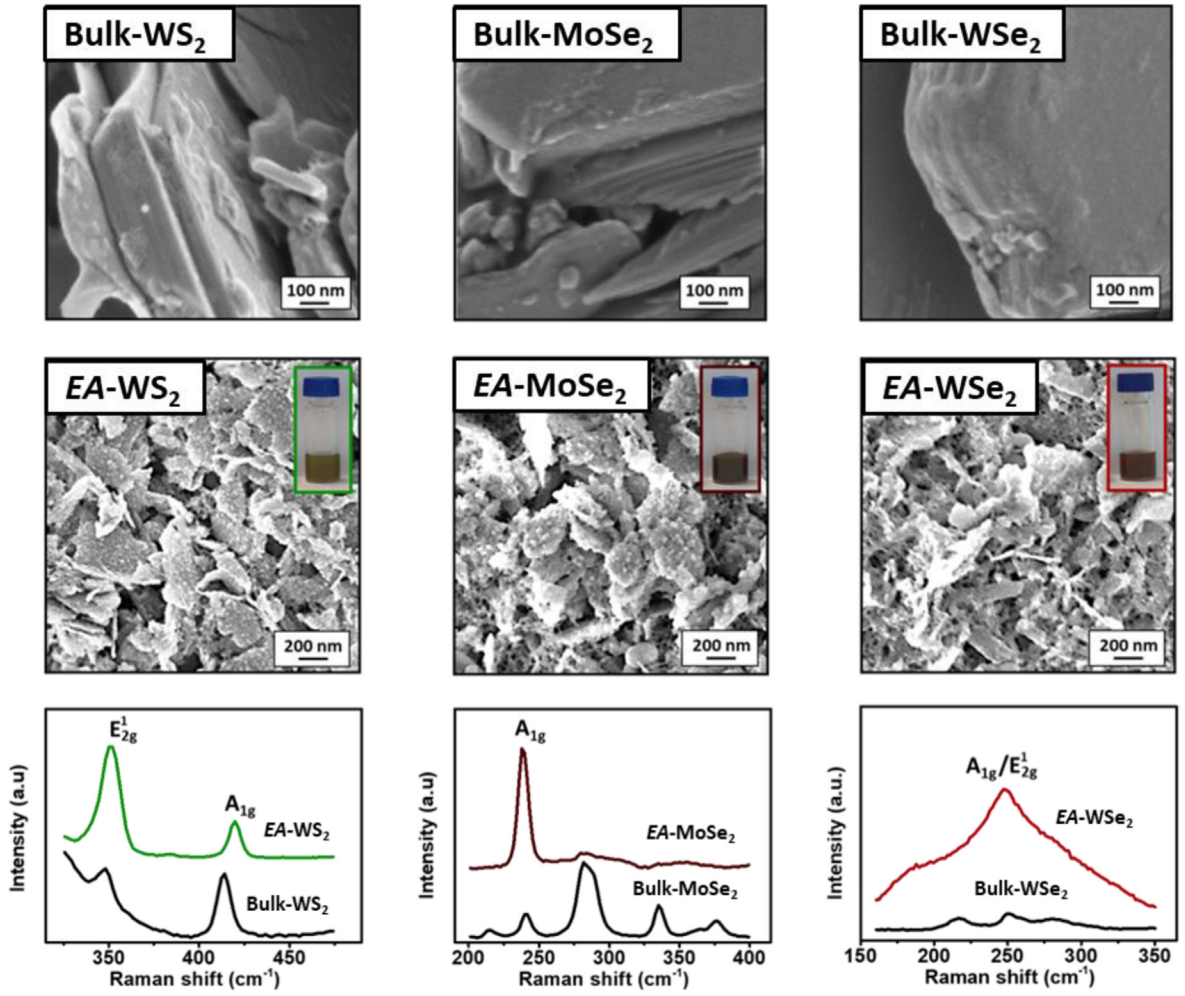

Fig. 7. SEM micrographs at the same magnification (100 kX) of the native WS_2 (bulk-WS_2), $MoSe_2$ (bulk-$MoSe_2$), and WSe_2 (bulk- WSe_2) and the respective EA exfoliated materials: *EA*-WS_2, *EA*-$MoSe_2$, and *EA*-WSe_2. The insets report the picture of the respective colloidal solutions. Raman spectra of the exfoliated TMDs against the respective native bulk materials (before exfoliation). SEM, scanning electron microscopy; TMD, transition metal chalcogenide.

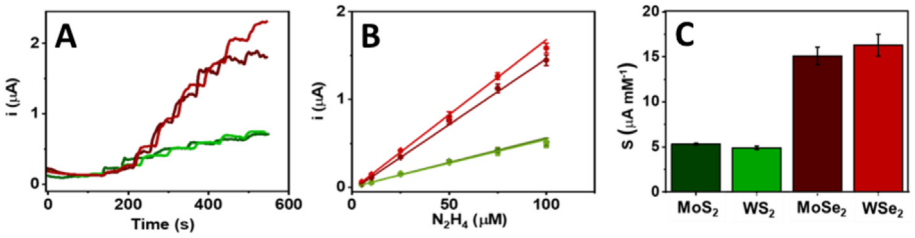

Fig. 8. (**a**) Amperometric signal for the calibration of the group VI *EA*-TMDs at different concentrations. (**b**) Calibration plots of the different EA-TMDs. Each point of the calibration plots has been tested in triplicate, RSD ≤8%. (**c**) Bar graph of the different sensitivities obtained (RSD ≤7%, n = 3). Overpotential used +0.4 V. EA, ellagic acid; TMD, transition metal chalcogenide.

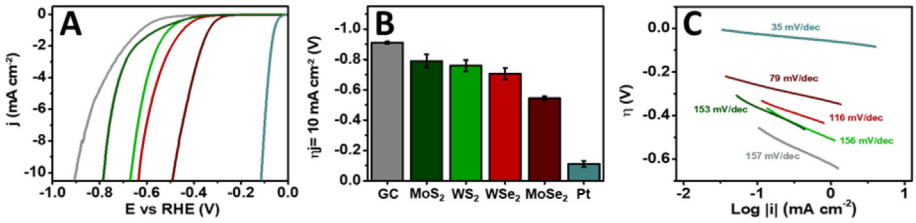

Fig. 9. (**a**) Linear sweep voltammetry for the HER reaction on the different electrodes: GC (gray), MoS_2 (dark green), WS_2 (light green), WSe_2 (red), $MoSe_2$ (brown) and Pt (navy). (**b**) Overpotentials required to obtain a geometrical current density of 10 mA cm^{-2}. Data reported as mean value of n = 3 repetitions, RSD ≤6%. (**c**) Tafel plots for the HER. Conditions: background electrolyte, H_2SO_4 (0.5 M) at scan rate, 5 mV s^{-1}. All measurements are performed relative to the Ag/AgCl reference electrode and transformed to reversible hydrogen electrode potentials. (For interpretation of the references to color in this figure legend, the reader is referred to the Web version of this article.) HER, hydrogen evolution reaction.

MoS_2, was also obtained for WS_2, $MoSe_2$, and WSe_2 as reported in Fig. S7. The success of the exfoliation process can be observed in the SEM micrographs in Fig. 7.

In all cases, a remarkable reduction of the lateral size of the flakes compared to the bulk material was observed, as well as an increase in the surface roughness is evident. Additionally, the Raman spectra of the different bulks and exfoliated materials are reported in Fig. 7. For all the materials, the characteristic vibration modes are visible; as for MoS_2, a blue shift is observed for the exfoliated materials which can be attributed to the successful exfoliation of the nanosheets [71].

The electrochemistry of the different group VI TMDs was also evaluated using the $[Fe(CN)_6]^{4-/3-}$. Fig. S8 shows the values of k^0 and $R_{CT.}$ The order of the electrochemical performance is the following: *EA*-$MoSe_2$ > *EA*-WSe_2 > *EA*-WS_2. All the three exfoliated materials exhibited improved performances in comparison with the previously discussed *EA*-MoS_2. This difference can be attributed to the different coverages of EA in the different materials and also, as previously reported by our group, by the different intrinsic performances of the TMD compound [72].

The intrinsic electrochemistry of EA was also transferred to the TMDs as shown in Fig. S9, as well as their ability to electrocatalyze N_2H_4 oxidation. For further comparison, the materials were tested in amperometric mode applying +0.4 V fixed potential (Fig. 8).

The performance in the N_2H_4 oxidation follows the trend WSe_2 ~ $MoSe_2$ > WS_2 ~ MoS_2 in agreement with the data obtained for the $[Fe(CN)_6]^{4-/3-}$ redox probe.

3.5. Electrochemistry of group VI TMDs. Hydrogen evolution reaction

The HER is the cathodic reaction in electrochemical water splitting, that, combined with renewable energy sources, leads to a sustainable source of hydrogen that can be used as an energy vector to both store energy during peak production and drive fuel cells. Research into MoS_2 as HER electrocatalyst has gained much interest in the last decade due to their good electrochemical performance, high abundance, and low cost; MoS_2 is considered a promising candidate to substitute noble metal-based electrodes [73,74]. The ability of the different materials obtained with our proposed LPE *EA*-assisted method in the HER was tested. Fig. 9A reports the HER polarization curves of the studied TMDs. A Pt and bare GC electrodes were added as controls.

Fig. 9B collects the overpotentials values obtained at a current density of 10 mA cm^{-2} which elect the $MoSe_2$ as the most promising material, exhibiting an overpotential value of 547 ± 13 mV followed by WS_2 with 757 ± 37 mV, WSe_2 with 707 ± 39 mV, and MoS_2 with 788 ± 42 mV. The same trend is obtained in the Tafel slopes (Fig. 9C) values being 79 ± 4, 116 ± 9, 156 ± 13, and 153 ± 11 mV dec^{-1} for $MoSe_2$, WS_2, WSe_2 and MoS_2, respectively. The GC electrode exhibits a poorer performance (998 ± 8 mV and 157 ± 3 $mVdec^{-1}$) demonstrating the ability of the different materials to catalyze the HER, whereas the Pt electrode exhibits the highest performance (104 ± 20 mV and 35 ± 2 mV dec^{-1}), with values in agreement with the literature [75]. The values obtained for the produced materials follow the same trend already reported in the literature for sodium cholate-assisted LPE [76].

4. Conclusions

In this work, we have systematically studied the ability of natural PCs to assist the exfoliation of group VI TMDs generating hybrid redox-active structures with improved electrochemical and catalytic activity. The changes in the TMDs electrochemistry can be attributed to the TMDs surface modification given by PCs, able to bring charges and redox-active moieties. EA results to be the best performing PC in terms of exfoliation yield and the transfer of electrochemical properties of PCs to TMDs. EA-based TMDs demonstrate to be able to electrocatalyze N_2H_4 oxidation and HER, with $MoSe_2$ as the most promising material paving the way for the use of these hybrid materials in analytical and energy-related applications. This work demonstrated for the first time the dual role of PCs, generally found in food, to act as exfoliating agents and as redox-active molecules, able to modify the electrocatalytic properties of the hybrid TMDs in contrast to classical surfactants employed in LPE. The *PC*-assisted exfoliation allows boosting the

electrochemical behavior of TMDs in two relevant electrochemical reactions: hydrazine oxidation and hydrogen evolution reaction.

Credit author statement

Daniel Rojas: Conceptualization; Data curation; Formal analysis; Investigation; Visualization; Methodology; Writing – original draft; Writing – review & editing.

Flavio Della Pelle: Conceptualization; Data curation; Formal analysis; Investigation; Methodology; Project administration; Supervision; Visualization; Writing – original draft; Writing – review & editing.

Filippo Silveri: Data curation; Investigation; Methodology; Visualization; Writing – review & editing.

Giovanni Ferraro: Conceptualization; Data curation; Investigation; Methodology; Validation; Writing – original draft, Writing – review & editing.

Emiliano Fratini: Conceptualization; Data curation; Methodology; Validation; Writing – review & editing.

Dario Compagnone: Conceptualization; Funding acquisition; Project administration; Resources; Supervision; Writing – review & editing.

Declaration of competing interest

The authors declare that they have no known competing financial interests or personal relationships that could have appeared to influence the work reported in this paper.

Data availability

Data will be made available on request.

Acknowledgment

F.D.P. and D.C. acknowledge the Ministry of Education, University and Research (MIUR) and European Social Fund (ESF) for the PON R&I 2014–2020 program, action 1.2 'AIM: Attraction and International Mobility' (AIM1894039-3).

D.C. acknowledges the PRIN 2017 ACTUaL project of the Italian Ministry of Education, University and Research (MIUR).

G.F. and E.F. acknowledge Consorzio per lo sviluppo dei Sistemi a Grande Interfase (CSGI) and "Progetto Dipartimenti di Eccellenza 2018–2022" allocated to Department of Chemistry "Ugo Schiff" from MIUR, for financial support.

Appendix A. Supplementary data

Supplementary data to this article can be found online at https://doi.org/10.1016/j.mtchem.2022.101122.

References

[1] B. Guo, Q. lan Xiao, S. hao Wang, H. Zhang, 2D layered materials: synthesis, nonlinear optical properties, and device applications, Laser Photon. Rev. 13 (2019) 1–46, https://doi.org/10.1002/lpor.201800327.

[2] X. Zhou, X. Hu, J. Yu, S. Liu, Z. Shu, Q. Zhang, H. Li, Y. Ma, H. Xu, T. Zhai, 2D layered material-based van der Waals heterostructures for optoelectronics, Adv. Funct. Mater. 28 (2018) 1–28, https://doi.org/10.1002/adfm.201706587.

[3] M. Samadi, N. Sarikhani, M. Zirak, H. Zhang, H.L. Zhang, A.Z. Moshfegh, Group 6 transition metal dichalcogenide nanomaterials: synthesis, applications and future perspectives, Nanoscale Horizons 3 (2018) 90–204, https://doi.org/10.1039/c7nh00137a.

[4] M. Xu, T. Liang, M. Shi, H. Chen, Graphene-like two-dimensional materials, Chem. Rev. 113 (2013) 3766–3798, https://doi.org/10.1021/cr300263a.

[5] M. Samadi, N. Sarikhani, M. Zirak, H. Zhang, H.L. Zhang, A.Z. Moshfegh, Group 6 transition metal dichalcogenide nanomaterials: synthesis, applications and future perspectives, Nanoscale Horizons 3 (2018) 90–204, https://doi.org/10.1039/c7nh00137a.

[6] M. Chhowalla, H.S. Shin, G. Eda, L.-J. Li, K.P. Loh, H. Zhang, The chemistry of two-dimensional layered transition metal dichalcogenide nanosheets, Nat. Chem. 5 (2013) 263–275, https://doi.org/10.1038/nchem.1589.

[7] E.P. Nguyen, T. Daeneke, S. Zhuiykov, K. Kalantar-Zadeh, Liquid exfoliation of layered transition metal dichalcogenides for biological applications, Curr Protoc Chem Biol 8 (2016) 97–108, https://doi.org/10.1002/cpch.3.

[8] E.D. Grayfer, M.N. Kozlova, V.E. Fedorov, Colloidal 2D nanosheets of MoS2 and other transition metal dichalcogenides through liquid-phase exfoliation, Adv. Colloid Interface Sci. 245 (2017) 40–61, https://doi.org/10.1016/j.cis.2017.04.014.

[9] X. Chia, M. Pumera, Layered transition metal dichalcogenide electrochemistry: journey across the periodic table, Chem. Soc. Rev. 47 (2018) 5602–5613, https://doi.org/10.1039/c7cs00846e.

[10] Z. Gholamvand, D. McAteer, A. Harvey, C. Backes, J.N. Coleman, Electrochemical applications of two-dimensional nanosheets: the effect of nanosheet length and thickness, Chem. Mater. 28 (2016) 2641–2651, https://doi.org/10.1021/acs.chemmater.6b00009.

[11] E.D. Grayfer, M.N. Kozlova, V.E. Fedorov, Colloidal 2D nanosheets of MoS2 and other transition metal dichalcogenides through liquid-phase exfoliation, Adv. Colloid Interface Sci. 245 (2017) 40–61, https://doi.org/10.1016/j.cis.2017.04.014.

[12] Q. Zhang, L. Mei, X. Cao, Y. Tang, Z. Zeng, Intercalation and exfoliation chemistries of transition metal dichalcogenides, J. Mater. Chem. 8 (2020) 15417–15444, https://doi.org/10.1039/d0ta03727c.

[13] C. Backes, T.M. Higgins, A. Kelly, C. Boland, A. Harvey, D. Hanlon, J.N. Coleman, Guidelines for exfoliation, characterization and processing of layered materials produced by liquid exfoliation, Chem. Mater. 29 (2017) 243–255, https://doi.org/10.1021/acs.chemmater.6b03335.

[14] A. Jawaid, D. Nepal, K. Park, M. Jespersen, A. Qualley, P. Mirau, L.F. Drummy, R.A. Vaia, Mechanism for liquid phase exfoliation of MoS2, Chem. Mater. 28 (2016) 337–348, https://doi.org/10.1021/acs.chemmater.5b04224.

[15] J.N. Coleman, M. Lotya, A. O'neill, S.D. Bergin, P.J. King, U. Khan, K. Young, A. Gaucher, S. De, R.J. Smith, I. V Shvets, S.K. Arora, G. Stanton, H.-Y. Kim, K. Lee, G.T. Kim, G.S. Duesberg, T. Hallam, J.J. Boland, J.J. Wang, J.F. Donegan, J.C. Grunlan, G. Moriarty, A. Shmeliov, R.J. Nicholls, J.M. Perkins, E.M. Grieveson, K. Theuwissen, D.W. Mccomb, P.D. Nellist, V. Nicolosi, Two-dimensional nanosheets produced by liquid exfoliation of layered material, Science 331 (1979) 568–571, 2011.

[16] A. Griffin, K. Nisi, J. Pepper, A. Harvey, B.M. Szydłowska, J.N. Coleman, C. Backes, Effect of surfactant choice and concentration on the dimensions and yield of liquid-phase-exfoliated nanosheets, Chem. Mater. 32 (2020) 2852–2862, https://doi.org/10.1021/acs.chemmater.9b04684.

[17] DESA, U.N., Transforming Our World: the 2030 Agenda for Sustainable Development, 2016.

[18] F. Arduini, L. Micheli, V. Scognamiglio, V. Mazzaracchio, D. Moscone, Sustainable materials for the design of forefront printed (bio)sensors applied in agrifood sector, TrAC, Trends Anal. Chem. 128 (2020), 115909, https://doi.org/10.1016/j.trac.2020.115909.

[19] T. Naghdi, S. Faham, T. Mahmoudi, N. Pourreza, R. Ghavami, H. Golmohammadi, Phytochemicals toward green (Bio)sensing, ACS Sens. 5 (2020) 3770–3805, https://doi.org/10.1021/acssensors.0c02101.

[20] R.K. Mishra, S.K. Ha, K. Verma, S.K. Tiwari, Recent progress in selected bio-nanomaterials and their engineering applications: an overview, J. Sci.: Advanced Materials and Devices 3 (2018) 263–288, https://doi.org/10.1016/j.jsamd.2018.05.003.

[21] J.I. Paredes, S. Villar-Rodil, Biomolecule-assisted exfoliation and dispersion of graphene and other two-dimensional materials: a review of recent progress and applications, Nanoscale 8 (2016) 15389–15413, https://doi.org/10.1039/c6nr02039a.

[22] B. Qurat Ul Ain, F. Silveri, F. Della Pelle, A. Scroccarello, D. Zappi, E. Cozzoni, D. Compagnone, Water-phase exfoliated biochar nano fi bers from Eucalyptus scraps for electrode modi fi cation and conductive film fabrication, ACS Sustain. Chem. Eng. 9 (2021) 13988–13998, https://doi.org/10.1021/acssuschemeng.1c05893.

[23] J. Guo, T. Suma, J.J. Richardson, H. Ejima, Modular assembly of biomaterials using polyphenols as building blocks, ACS Biomater. Sci. Eng. 5 (2019) 5578–5596, https://doi.org/10.1021/acsbiomaterials.8b01507.

[24] A. Scroccarello, F. Della Pelle, G. Ferraro, E. Fratini, F. Tempera, E. Dainese, D. Compagnone, Plasmonic active film integrating gold/silver nanostructures for H2O2 readout, Talanta 222 (2021), 121682, https://doi.org/10.1016/j.talanta.2020.121682.

[25] A. Scroccarello, B. Molina-Hernández, F. Della Pelle, J. Ciancetta, G. Ferraro, E. Fratini, L. Valbonetti, C. Chaves Copez, D. Compagnone, Effect of phenolic compounds-capped AgNPs on growth inhibition of Aspergillus Niger, Colloids Surf. B Biointerfaces 199 (2021), 111533, https://doi.org/10.1016/j.colsurfb.2020.111533.

[26] J. Saiz-Poseu, J. Mancebo-Aracil, F. Nador, F. Busqué, D. Ruiz-Molina, The chemistry behind catechol-based adhesion, Angew. Chem., Int. Ed. 58 (2019) 696–714, https://doi.org/10.1002/anie.201801063.

[27] J. Zhou, Z. Lin, Y. Ju, A. Rahim, J.J. Richardson, F. Caruso, Polyphenol-mediated assembly for particle engineering, Acc. Chem. Res. 53 (2020) 1269–1278, https://doi.org/10.1021/acs.accounts.0c00150.

[28] J. Guo, T. Suma, J.J. Richardson, H. Ejima, Modular assembly of biomaterials using polyphenols as building blocks, ACS Biomater. Sci. Eng. 5 (2019) 5578–5596, https://doi.org/10.1021/acsbiomaterials.8b01507.
[29] D. Hou, Q. Liu, H. Cheng, K. Li, D. Wang, H. Zhang, Chrysanthemum extract assisted green reduction of graphene oxide, Mater. Chem. Phys. 183 (2016) 76–82, https://doi.org/10.1016/j.matchemphys.2016.08.004.
[30] Y. Xu, H. Cao, Y. Xue, B. Li, W. Cai, Liquid-phase exfoliation of graphene: an overview on exfoliation media, techniques, and challenges, Nanomaterials 8 (2018), https://doi.org/10.3390/nano8110942.
[31] A. Ciesielski, P. Samorì, Supramolecular approaches to graphene: from self-assembly to molecule-assisted liquid-phase exfoliation, Adv. Mater. 28 (2016) 6030–6051, https://doi.org/10.1002/adma.201505371.
[32] F. Silveri, F. Della Pelle, D. Rojas, G. Ferraro, Q.U.A. Bukhari, E. Fratini, D. Compagnone, (+)-Catechin-assisted graphene production by sonochemical exfoliation in water. A new redox-active nanomaterial for electromediated sensing, Microchim. Acta 188 (2021) 369, https://doi.org/10.1007/s00604-021-05018-2.
[33] S. Ravula, J.B. Essner, G.A. Baker, Kitchen-inspired nanochemistry: dispersion, exfoliation, and hybridization of functional MoS2 nanosheets using culinary hydrocolloids, ChemNanoMat 1 (2015) 167–177, https://doi.org/10.1002/cnma.201500022.
[34] C. Zhang, D.F. Hu, J.W. Xu, M.Q. Ma, H. Xing, K. Yao, J. Ji, Z.K. Xu, Polyphenol-assisted exfoliation of transition metal dichalcogenides into nanosheets as photothermal nanocarriers for enhanced antibiofilm activity, ACS Nano 12 (2018) 12347–12356, https://doi.org/10.1021/acsnano.8b06321.
[35] M.Q. Ma, C. Zhang, C.Y. Zhu, S. Huang, J. Yang, Z.K. Xu, Nanocomposite membranes embedded with functionalized MoS2 nanosheets for enhanced interfacial compatibility and nanofiltration performance, J. Membr. Sci. 591 (2019), 117316, https://doi.org/10.1016/j.memsci.2019.117316.
[36] H. Zhao, H. Wu, J. Wu, J. Li, Y. Wang, Y. Zhang, H. Liu, Preparation of MoS2/WS2 nanosheets by liquid phase exfoliation with assistance of epigallocatechin gallate and study as an additive for high-performance lithium-sulfur batteries, J. Colloid Interface Sci. 552 (2019) 554–562, https://doi.org/10.1016/j.jcis.2019.05.080.
[37] H. Peng, D. Wang, S. Fu, Tannic acid-assisted green exfoliation and functionalization of MoS2 nanosheets: significantly improve the mechanical and flame-retardant properties of polyacrylonitrile composite fibers, Chem. Eng. J. 384 (2020), 123288, https://doi.org/10.1016/j.cej.2019.123288.
[38] C.C. Hsueh, C.C. Wu, B.Y. Chen, Polyphenolic compounds as electron shuttles for sustainable energy utilization, Biotechnol. Biofuels 12 (2019) 1–26, https://doi.org/10.1186/s13068-019-1602-9.
[39] L.V. da Silva, A.K.A. de Almeida, J.A. Xavier, C.B. Lopes, F.D.A. dos Santos Silva, P.R. Lima, N.D. dos Santos, L.T. Kubota, M.O.F. Goulart, Phenol based redox mediators in electroanalysis, J. Electroanal. Chem. 827 (2018) 230–252, https://doi.org/10.1016/j.jelechem.2018.05.027.
[40] F. Della Pelle, L. Blandón-Naranjo, M. Alzate, M. Del Carlo, D. Compagnone, Cocoa powder and catechins as natural mediators to modify carbon-black based screen-printed electrodes. Application to free and total glutathione detection in blood, Talanta 207 (2020), 120349, https://doi.org/10.1016/j.talanta.2019.120349.
[41] F. Silveri, F. Della Pelle, D. Rojas, G. Ferraro, Q.U.A. Bukhari, E. Fratini, D. Compagnone, (+)-Catechin-assisted graphene production by sonochemical exfoliation in water. A new redox-active nanomaterial for electromediated sensing, Microchim. Acta 188 (2021) 369, https://doi.org/10.1007/s00604-021-05018-2.
[42] A.C. Fonseca, M.S. Lima, A.F. Sousa, A.J. Silvestre, J.F.J. Coelho, A.C. Serra, Cinnamic acid derivatives as promising building blocks for advanced polymers: synthesis, properties and applications, Polym. Chem. 10 (2019) 1696–1723, https://doi.org/10.1039/c9py00121b.
[43] P. Pinho, O. Ferreira, Solubility of flavonoids in pure and mixed solvents, Ind. Eng. Chem. Res. 51 (2012) 6586–6590.
[44] F.L. Mota, A.J. Queimada, S.P. Pinho, E.A. Macedo, Aqueous solubility of some natural phenolic compounds, Ind. Eng. Chem. Res. 47 (2008) 5182–5189, https://doi.org/10.1021/ie071452o.
[45] A. Scroccarello, F. Della Pelle, E. Fratini, G. Ferraro, S. Scarano, P. Palladino, D. Compagnone, Colorimetric determination of polyphenols via a gold nanoseeds–decorated polydopamine film, Microchim. Acta 187 (2020) 1–10, https://doi.org/10.1007/s00604-020-04228-4.
[46] S. Muráth, A. Szerlauth, D. Sebők, I. Szilágyi, Layered double hydroxide nanoparticles to overcome the hydrophobicity of ellagic acid: an antioxidant hybrid material, Antioxidants 9 (2020), https://doi.org/10.3390/antiox9020153.
[47] D.D. Evtyugin, S. Magina, D.V. Evtuguin, Recent advances in the production and applications of ellagic acid and its derivatives, A Review, Molecules 25 (2020), https://doi.org/10.3390/molecules25122745.
[48] A.S. Kumar, R. Shanmugam, N. Vishnu, K.C. Pillai, S. Kamaraj, Electrochemical immobilization of ellagic acid phytochemical on MWCNT modified glassy carbon electrode surface and its efficient hydrazine electrocatalytic activity in neutral pH, J. Electroanal. Chem. 782 (2016) 215–224, https://doi.org/10.1016/j.jelechem.2016.10.010.
[49] D.D. Evtyugin, S. Magina, D.V. Evtuguin, Recent advances in the production and applications of ellagic acid and its derivatives, A Review, Molecules 25 (2020), https://doi.org/10.3390/molecules25122745.
[50] J. Saiz-Poseu, J. Mancebo-Aracil, F. Nador, F. Busqué, D. Ruiz-Molina, The chemistry behind catechol-based adhesion, Angew. Chem., Int. Ed. 58 (2019) 696–714, https://doi.org/10.1002/anie.201801063.
[51] T. Sander, J. Freyss, M. von Korff, C. Rufener, DataWarrior: an open-source program for chemistry aware data visualization and analysis, J. Chem. Inf. Model. 55 (2015) 460–473, https://doi.org/10.1021/CI500588J/ASSET/IMAGES/MEDIUM/CI-2014-00588J_0016. GIF.
[52] S. Muráth, A. Szerlauth, D. Sebők, I. Szilágyi, Layered double hydroxide nanoparticles to overcome the hydrophobicity of ellagic acid: an antioxidant hybrid material, Antioxidants 9 (2020), https://doi.org/10.3390/antiox9020153.
[53] T. Sander, J. Freyss, M. Von Korff, C. Rufener, DataWarrior: an open-source program for chemistry aware data visualization and analysis, J. Chem. Inf. Model. 55 (2015) 460–473, https://doi.org/10.1021/ci500588j.
[54] G. Eda, S.A. Maier, Two-dimensional crystals: managing light for optoelectronics, ACS Nano 7 (2013) 5660–5665, https://doi.org/10.1021/nn403159y.
[55] N. Dong, Y. Li, Y. Feng, S. Zhang, X. Zhang, C. Chang, J. Fan, L. Zhang, J. Wang, Optical limiting and theoretical modelling of layered transition metal dichalcogenide nanosheets, Sci. Rep. 5 (2015), 14646, https://doi.org/10.1038/srep14646.
[56] A. Molina-Sánchez, L. Wirtz, Phonons in single-layer and few-layer MoS2 and WS2, Phys. Rev. B Condens. Matter 84 (2011), 155413, https://doi.org/10.1103/PhysRevB.84.155413.
[57] H. Ma, S. Ben, Z. Shen, X. Zhang, C. Wu, S. Liao, F. An, Investigating the exfoliation behavior of MoS2 and graphite in water: a comparative study, Appl. Surf. Sci. 512 (2020), 145588, https://doi.org/10.1016/j.apsusc.2020.145588.
[58] S.K. Bhangu, R. Singla, E. Colombo, M. Ashokkumar, F. Cavalieri, Sono-transformation of tannic acid into biofunctional ellagic acid micro/nanocrystals with distinct morphologies, Green Chem. 20 (2018) 816–821, https://doi.org/10.1039/c7gc03163g.
[59] X. Huang, Q. Shi, S. Du, Y. Lu, N. Han, Poly-tannic acid coated paclitaxel nanocrystals for combinational photothermal-chemotherapy, Colloids Surf. B Biointerfaces 197 (2021), 111377, https://doi.org/10.1016/j.colsurfb.2020.111377.
[60] S.K. Bhangu, M. Ashokkumar, F. Cavalieri, A simple one-step ultrasonic route to synthesize antioxidant molecules and fluorescent nanoparticles from phenol and phenol-like molecules, ACS Sustain. Chem. Eng. 5 (2017) 6081–6089, https://doi.org/10.1021/acssuschemeng.7b00966.
[61] A. Guiberteau-Cabanillas, B. Godoy-Cancho, E. Bernalte, M. Tena-Villares, C. GuiberteauCabanillas, M.A. Martínez-Cañas, Electroanalytical behavior of gallic and ellagic acid using graphene modified screen-printed electrodes. Method for the determination of total low oxidation potential phenolic compounds content in cork boiling waters, Electroanalysis 27 (2015) 177–184, https://doi.org/10.1002/elan.201400418.
[62] P. Janeiro, A.M.O. Brett, Solid state electrochemical oxidation mechanisms of morin in aqueous media, Electroanalysis 17 (2005) 733–738, https://doi.org/10.1002/elan.200403155.
[63] P. Janeiro, A.M. Oliveira Brett, Catechin electrochemical oxidation mechanisms, Anal. Chim. Acta 518 (2004) 109–115, https://doi.org/10.1016/j.aca.2004.05.038.
[64] B.L. Hanssen, S. Siraj, D.K.Y. Wong, Recent strategies to minimise fouling in electrochemical detection systems, Rev. Anal. Chem. 35 (2016) 1–28, https://doi.org/10.1515/revac-2015-0008.
[65] X. Liu, S. You, F. Ma, H. Zhou, Characterization of electrode fouling during electrochemical oxidation of phenolic pollutant, Front. Environ. Sci. Eng. 15 (2021) 1–10, https://doi.org/10.1007/s11783-020-1345-7.
[66] F. Della Pelle, D. Rojas, A. Scroccarello, M. Del Carlo, G. Ferraro, C. Di Mattia, M. Martuscelli, A. Escarpa, D. Compagnone, High-performance carbon black/molybdenum disulfide nanohybrid sensor for cocoa catechins determination using an extraction-free approach, Sensor. Actuator. B Chem. 296 (2019), 126651, https://doi.org/10.1016/j.snb.2019.126651.
[67] P. Chen, R.L. McCreery, Control of electron transfer kinetics at glassy carbon electrodes by specific surface modification, Anal. Chem. 68 (1996) 3958–3965, https://doi.org/10.1021/ac960492r.
[68] J. Panchompoo, L. Aldous, C. Downing, A. Crossley, R.G. Compton, Facile synthesis of pd nanoparticle modified carbon black for electroanalysis: application to the detection of hydrazine, Electroanalysis 23 (2011) 1568–1578, https://doi.org/10.1002/elan.201100163.
[69] P. Swetha, K.S.S. Devi, A.S. Kumar, In-situ trapping and confining of highly redox active quinoline quinones on MWCNT modified glassy carbon electrode and its selective electrocatalytic oxidation and sensing of hydrazine, Electrochim. Acta 147 (2014) 62–72, https://doi.org/10.1016/j.electacta.2014.08.128.
[70] A. Serov, C. Kwak, Direct hydrazine fuel cells: a review, Appl. Catal. B Environ. 98 (2010) 1–9, https://doi.org/10.1016/j.apcatb.2010.05.005.
[71] H. Ma, S. Ben, Z. Shen, X. Zhang, C. Wu, S. Liao, F. An, Investigating the exfoliation behavior of MoS2 and graphite in water: a comparative study, Appl. Surf. Sci. 512 (2020), 145588, https://doi.org/10.1016/j.apsusc.2020.145588.
[72] D. Rojas, F. Della Pelle, M. Del Carlo, D. Compagnone, A. Escarpa, Group VI transition metal dichalcogenides as antifouling transducers for electrochemical oxidation of catechol-containing structures, Electrochem. Commun. 115 (2020), 106718, https://doi.org/10.1016/j.elecom.2020.106718.
[73] G. Zhang, H. Liu, J. Qu, J. Li, Two-dimensional layered MoS2: rational design, properties and electrochemical applications, Energy Environ. Sci. 9 (2016) 1190–1209, https://doi.org/10.1039/C5EE03761A.
[74] T.F. Jaramillo, K.P. Jørgensen, J. Bonde, J.H. Nielsen, S. Horch, I. Chorkendorff, Identification of active edge sites for electrochemical H2 evolution from

MoS2 nanocatalysts, Science (2007) 100–102, https://doi.org/10.1126/SCIENCE.1141483/SUPPL_FILE/JARAMILLO_SOM.PDF (1979). 317.
[75] B.E. Conway, B.V. Tilak, Interfacial processes involving electrocatalytic evolution and oxidation of H2, and the role of chemisorbed H, Electrochim. Acta 47 (2002) 3571–3594, https://doi.org/10.1016/S0013-4686(02)00329-8.
[76] Z. Gholamvand, D. McAteer, C. Backes, N. McEvoy, A. Harvey, N.C. Berner, D. Hanlon, C. Bradley, I. Godwin, A. Rovetta, M.E.G. Lyons, G.S. Duesberg, J.N. Coleman, Comparison of liquid exfoliated transition metal dichalcogenides reveals MoSe2to be the most effective hydrogen evolution catalyst, Nanoscale 8 (2016) 5737–5749, https://doi.org/10.1039/c5nr08553e.